Exchange coupling and magnetic anisotropy at Fe/FePt interfaces

C. J. Aas,[1] P. J. Hasnip,[1] R. Cuadrado,[1] E. M. Plotnikova,[1] L. Szunyogh,[2,3] L. Udvardi,[2,3] and R. W. Chantrell[1]

[1]*Department of Physics, University of York, York YO10 5DD, United Kingdom*

[2]*Department of Theoretical Physics, Budapest University of Technology and Economics, Budafoki út 8, H-1111 Budapest, Hungary*

[3]*Condensed Matter Research Group of Hungarian Academy of Sciences, Budapest University of Technology and Economics, Budafoki út 8, H-1111 Budapest, Hungary*

(Received 13 June 2013; published 13 November 2013)

We perform fully relativistic first-principles calculations of the exchange interactions and the magnetocrystalline anisotropy energy (MAE) in an Fe/FePt/Fe sandwich system in order to elucidate how the presence of Fe/FePt (soft/hard magnetic) interfaces impacts on the magnetic properties of Fe/FePt/Fe multilayers. Throughout our study we make comparisons between a geometrically unrelaxed system and a geometrically relaxed system. We observe that the Fe layer at the Fe/FePt interface plays a crucial role inasmuch as its (isotropic) exchange coupling to the soft (Fe) phase of the system is substantially reduced. Moreover, this interfacial Fe layer has a substantial impact on the MAE of the system. We show that the MAE of the FePt slab, including the contribution from the Fe/FePt interface, is dominated by anisotropic intersite exchange interactions. Our calculations indicate that the change in the MAE of the FePt slab with respect to the corresponding bulk value is negative, i.e., the presence of Fe/FePt interfaces appears to reduce the perpendicular MAE of the Fe/FePt/Fe system. However, for the relaxed system, this reduction is marginal. It is also shown that the relaxed system exhibits a reduced interfacial exchange. Using a simple linear chain model, we demonstrate that the reduced exchange leads to a discontinuity in the magnetization structure at the interface.

DOI: 10.1103/PhysRevB.88.174409 PACS number(s): 75.30.Gw, 75.50.Ss, 71.15.Mb, 75.30.Et

I. INTRODUCTION

Exchange-coupled soft/hard composite magnetic systems are of significant interest for their potential application in many different fields of technology such as magnetic recording media,[1] permanent magnets,[2] and magnetic microactuators.[3] A wealth of different soft/hard materials has been investigated in the literature (see, e.g., Refs. 4–10). Experimentally, the Fe/FePt system is a highly suitable system for studying the fundamental properties of nanocomposite magnetic systems as the properties are relatively easy to control.[11] Moreover, due to the high magnetization of the saturated α-Fe phase and the large magnetocrystalline anisotropy energy (MAE) of the FePt $L1_0$ phase, Fe/FePt bilayers are considered an ideal structure for exchange spring behavior[12] and for application in exchange-coupled composite (ECC) magnetic recording media. For ECC applications, the (soft) Fe phase, through its exchange interaction with the (hard) FePt phase, would act as a lever, reducing the write field. Meanwhile, the thermal stability of the written information would be ensured by the large MAE of $L1_0$ FePt. Thus, in order to realize such devices, the MAE of FePt needs to be maintained (if possible, enhanced). The effect of the Fe/FePt interface on the FePt MAE is therefore a very important aspect.

The aim of the present work is to investigate in detail the effect of the Fe/FePt interface on the exchange coupling and the MAE of an Fe/FePt/Fe system by means of first-principles calculations. We compare the results of a geometrically relaxed Fe/FePt/Fe system to the corresponding results for an unrelaxed system. The latter is similar to the system studied by Sabiryanov and Jaswal.[13] We use the CASTEP code[14–16] to obtain the relaxed ionic coordinates of an Fe/FePt/Fe system. We then employ the fully relativistic screened Korringa-Kohn-Rostoker (SKKR) method[17] (see Sec. II) to calculate tensorial exchange interactions and the layer-resolved contributions to the MAE of the relaxed and unrelaxed Fe/FePt/Fe structures. Moreover, we evaluate the change in the FePt MAE induced by the presence of the Fe/FePt interfaces.

Not only is such a study important from the point of view of understanding the properties of this nanocomposite, but the site-resolved information is also central to the development and parametrization of localized-spin models. This strategy has recently been realized to study an $IrMn_3$/Co(111) interface.[18] The exchange interactions and the on-site magnetic anisotropy constants have been calculated in the antiferromagnetic and ferromagnetic parts of the system, as well as at the interface between them, and then used in atomistic spin-dynamics simulations to investigate the exchange bias effect.[19] In particular, it was found that the exchange bias effect in this system is mainly governed by large Dzyaloshinskii-Moriya (DM) interactions[20,21] between the Mn and Co atoms at the interface.

We thus consider the implications of our calculated *ab initio* parameters in a multiscale modeling approach. Here one maps *ab initio* information onto a Heisenberg-type model of localized spins to allow calculations of thermodynamic quantities and magnetization dynamics. By further simplifying this mapping onto an effective spin Hamiltonian describing a linear chain, we study domain structures at the FePt/Fe interface using the *ab initio* parameters. Importantly, the *ab initio* calculations show that the relaxed system exhibits a reduced interfacial exchange coupling. Mapping this information onto the linear chain model shows that this reduction gives rise to a discontinuitylike feature in the domain wall structure at the FePt/Fe interface. The implications for the exchange spring effect are considered. The functionality of magnetic materials increasingly relies on structural design at the nanoscale, the exchange spring phenomenon, its use in permanent magnets and recording media being an excellent example. Mesoscopic

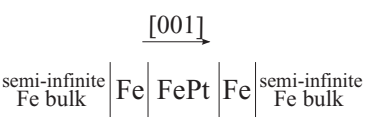

FIG. 1. Sketch of the Fe/FePt/Fe multilayer system as stacked in between two semi-infinite bcc Fe bulk systems along the (001) axis.

calculations often assume bulk exchange coupling across interfaces, which clearly may not be the case, and will certainly depend on the material properties in a way which can only be elucidated by electronic structure calculations.

II. DETAILS OF THE CALCULATIONS

First we describe the geometric structure of the Fe/FePt/Fe sandwich system that we have chosen for our investigation. The SKKR method requires the system to be considered in terms of an intermediate layer region (region I) positioned between two semi-infinite bulk regions. For region I, we considered a sequence of atomic layers (ALs) as sketched in Fig. 1 and detailed in Table I, namely, 7 Fe AL + 17 Pt/Fe/$\cdots$/Fe/Pt AL + 7 Fe AL, enclosed by two semi-infinite bulk Fe systems.

Using the layer sequence in Table I, we investigated the following two systems.

System A is a geometrically unrelaxed system with an overall two-dimensional lattice parameter $a_{2D} = a_{FePt}/\sqrt{2} \approx 2.723$ Å, where $a_{FePt} = 3.852$ Å is the experimental in-plane lattice parameter of the $L1_0$ lattice of FePt. Note that 2.723 Å is within 5% of the experimental lattice parameter of bcc Fe, $a_{Fe}^{(expt)} = 2.87$ Å. For the FePt part of the system we used the experimentally measured ratio of $c_{FePt}/a_{FePt} = 0.964$, while for the bcc Fe part, $c_{Fe} = a_{2D}$. At the interface between the Fe and FePt parts of the system, i.e., between ALs -9 and -10, as well as between ALs 9 and 10 (see Table I), we set the interlayer separation to

$$c_{interface} = \frac{c_{Fe} + c_{FePt}}{4}.$$

System B is a system in which the interlayer separations are relaxed using CASTEP.[14–16] CASTEP is a widely used electronic structure code based on plane-wave density-functional theory (DFT). The core electrons are treated using scalar-relativistic nonlinear core-corrected Vanderbilt ultrasoft pseudopotentials, with the valence electrons treated using a Kohn-Sham-Mermin functional and optimized using a preconditioned Davidson algorithm.[22] Here we choose $a_{2D} = a_{Fe}^{(LDA)}$, where $a_{Fe}^{(LDA)}$ is the bulk lattice parameter for Fe obtained using the localdensity approximation (LDA) in CASTEP, 2.659 Å. All the interatomic distances of the resulting relaxed structure were then scaled up by a uniform factor of 1.024 in order to match the experimental FePt lattice parameter $a_{2D} = 2.723$ Å and thus enable a direct comparison with the results for system A. It should be noted here that the CASTEP geometry relaxation yields an Fe region that is slightly tetragonal (rather than cubic), with the ratio $c_{Fe}/a_{Fe} \approx 1.06$. As this tetragonalization must be due to the presence of the FePt slab, the relaxed geometry of system B corresponds more closely to a repeated multilayer structure.

We should mention that we also investigated an unrelaxed sandwich system with a layout of (1 × 2) Fe/Pt AL + 9 Fe AL + 17 Pt/Fe/$\cdots$/Fe/Pt AL + 9 Fe AL + (1 × 2) Pt/Fe ALs enclosed by FePt bulk (system C). Since the considered Fe and FePt layers are quite thick, as expected, the magnetic properties (spin moments, exchange interactions, and MAE) of system C turned out very similar to those of system A. In this study, we used system C only for calibrating the change in the MAE of the FePt slab with respect to the MAE of bulk FePt.

For system B, after specifying the vertical coordinate z_p of each atomic layer p from the CASTEP geometry relaxation, we needed to determine the corresponding atomic volumes V_p. Here the only strict requirement is that the sum of atomic volumes within region I should be equal to the total lattice volume of region I, while the choice of the individual atomic volumes is somewhat arbitrary. As a simple choice, we related the atomic volume of each atom in layer p, V_p, to the layer positions $\{z_p\}$ as $V_p = a_{2D}^2(z_{p+1} - z_{p-1})/2$. For Fe or FePt bulk, this construction trivially retains the corresponding bulk atomic volumes. The values of Δz_p and the atomic radii S_p (defined through $V_p = \frac{4\pi}{3} S_p^3$) are shown in Table II for system A. The corresponding values for system B are displayed in Fig. 2.

For each of the systems A and B, we performed self-consistent calculations by means of the SKKR method.[17] Within the SKKR method, the one-electron Green's function of a layered system is evaluated, from which the charge and magnetization densities are calculated. We used the local spin-density approximation (LSDA) of the DFT as parametrized by Vosko *et al.*,[23] with effective potentials and fields treated within the atomic sphere approximation (ASA).

TABLE II. Interlayer separations $\Delta z_p = z_{p+1} - z_p$ for $p \geqslant 0$ and $\Delta z_p = z_p - z_{p-1}$ for $p < 0$ and the atomic sphere radii $S_p = a_{2D}\sqrt[3]{3\,\Delta z_p/4\pi}$, in system A. Note that the interlayer distances for bcc Fe and $L1_0$ FePt are $\Delta z_{Fe} = \frac{a_{2D}}{2}$ and $\Delta z_{FePt} = \frac{c}{a}\frac{a_{2D}}{\sqrt{2}}$ with $\frac{c}{a} = 0.964$, respectively, while at the interfaces we choose $\Delta z_{\pm 9} = (\Delta z_{Fe} + \Delta z_{FePt})/2$.

AL index p	Δz_p (a_{2D})	S_p (a_{2D})
±15	0.5	0.492
±10	0.5	0.492
±9	0.591	0.521
±8	0.681	0.546
±1	0.681	0.546
0	0.681	0.546

TABLE I. Numbering of the atomic layers in the 7 Fe AL + 17 Pt/Fe/$\cdots$/Fe/Pt AL + 7 Fe AL sandwich system. Underlines refer to the Fe layers at the interface between the Fe parts (soft magnet) and the FePt slab (hard magnet).

−15	$\cdots$	−11	−10	−9	−8	−7	−6	$\cdots$	−1	0	1	$\cdots$	6	7	8	9	10	11	$\cdots$	15
Fe	$\cdots$	Fe	Fe	Fe	Pt	Fe	Pt	$\cdots$	Fe	Pt	Fe	$\cdots$	Pt	Fe	Pt	Fe	Fe	Fe	$\cdots$	Fe

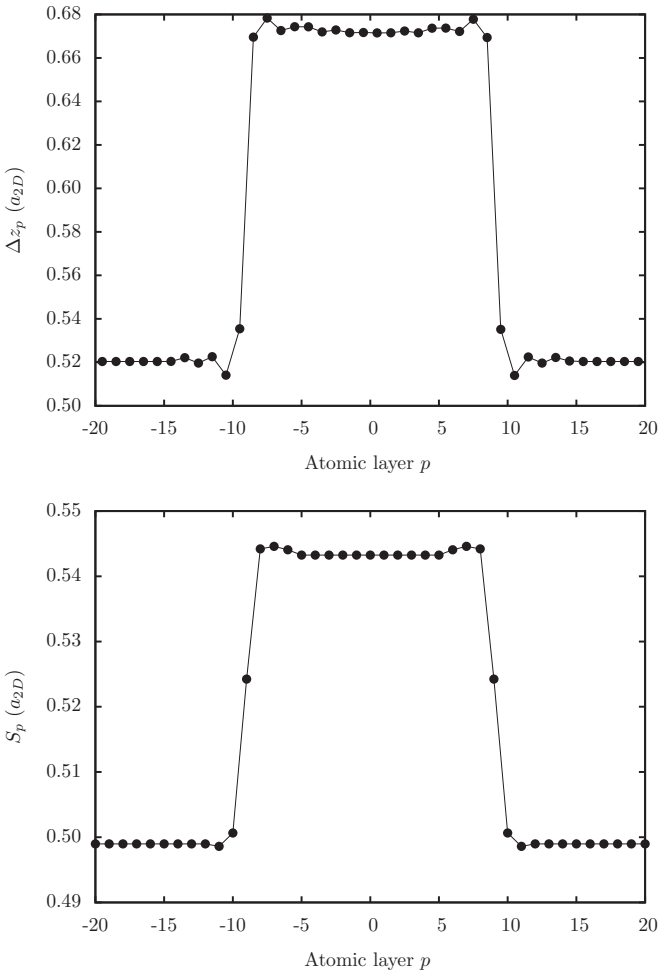

FIG. 2. Interlayer spacings Δz_p (top) and radii of atomic spheres S_p (bottom) as used for system B. Solid lines serve as guides for the eye.

The self-consistent calculations were performed within the scalar-relativistic approximation and an angular momentum cutoff $\ell_{\max} = 3$. A semicircular contour with 16 energy points was used for the necessary energy integrations. The imaginary part of the energy point closest to the Fermi level was below 10^{-4} Ry, thus Fermi level smearing effects can be neglected.

The MAE was then evaluated in terms of the fully relativistic SKKR method. Here we solved the Kohn-Sham-Dirac equation, i.e., we used the four-component Dirac formalism implying that the spin-orbit coupling is treated nonperturbatively. We used the magnetic force theorem,[24] in which the total energy of the system can be replaced by the single-particle (band) energy. Moreover, we employed the torque method,[25] making use of the fact that, for a uniaxial system, the MAE K can be calculated up to second order in spin-orbit coupling as

$$K = E(\theta = 90^\circ) - E(\theta = 0^\circ) = \left.\frac{dE}{d\theta}\right|_{\theta=45^\circ}, \qquad (1)$$

where θ denotes the angle of the magnetization direction with respect to the [001] direction of the FePt lattice. Within the Korringa-Kohn-Rostoker (KKR) formalism, K can be decomposed into site-resolved contributions K_i,

$$K = \sum_i K_i. \qquad (2)$$

For more details on the torque method within the KKR method see Ref. 26. We should emphasize that, unlike other approaches in the literature,[27,28] the site resolution of the MAE is based on a spatial decomposition of the density of states (DOS) (or Green's function). Due to the two-dimensional translational symmetry of the systems, K_i takes the same value for each site i within a given layer p, which we shall refer to as the layer-resolved MAE contribution K_p.

Having evaluated the layer-resolved contributions to the MAE for each Fe/FePt/Fe system, we considered next a multiscale approach of using our calculated parameters within a localized-spin model. Supposing that the electronic energy of a uniaxial magnetic system can be mapped into a generalized Heisenberg model

$$\mathcal{H} = -\frac{1}{2}\sum_{i,j(\neq i)} \vec{S}_i \boldsymbol{J}_{ij} \vec{S}_j - \sum_i d_i (\vec{S}_i \cdot \vec{e})^2, \qquad (3)$$

where $\vec{S}_i$ represents a classical spin, i.e., a unit vector along the direction of the magnetic moment at site i. The first term stands for the exchange contribution to the energy, with $\boldsymbol{J}_{ij}$ denoting the tensorial exchange interaction, and the second term denotes the on-site anisotropy, with the anisotropy constant d_i and the easy magnetic direction $\vec{e}$. The exchange interaction matrix $\boldsymbol{J}_{ij}$ can further be decomposed into three terms[29]

$$\boldsymbol{J}_{ij} = J_{ij}\boldsymbol{I} + \boldsymbol{J}^S_{ij} + \boldsymbol{J}^A_{ij}, \qquad (4)$$

with $J_{ij} = \frac{1}{3}\mathrm{Tr}\boldsymbol{J}_{ij}$ the isotropic exchange interaction, $\boldsymbol{J}^S_{ij} = \frac{1}{2}(\boldsymbol{J}_{ij} + \boldsymbol{J}^T_{ij}) - J^{\mathrm{iso}}_{ij}\boldsymbol{I}$ the traceless symmetric part of the exchange tensor, and $\boldsymbol{J}^A_{ij} = \frac{1}{2}(\boldsymbol{J}_{ij} - \boldsymbol{J}^T_{ij})$ the antisymmetric part of the exchange tensor.

Within the spin model [Eq. (3)] the MAE of a uniaxial ferromagnetic system can be cast into on-site and intersite parts

$$K = K_{\text{on-site}} + K_{\text{intersite}}, \qquad (5)$$

where

$$K_{\text{on-site}} = \sum_i d_i \qquad (6)$$

and

$$K_{\text{intersite}} = -\frac{1}{2}\sum_{i,j\ (\neq i)} \left(J^{xx}_{ij} - J^{zz}_{ij}\right). \qquad (7)$$

Defining thus the site-resolved intersite anisotropy as

$$K_{i,\text{intersite}} = -\frac{1}{2}\sum_{j(\neq i)} \left(J^{xx}_{ij} - J^{zz}_{ij}\right), \qquad (8)$$

the site-resolved MAE in Eq. (2) can be compared within the spin model to

$$K_i = d_i + K_{i,\text{intersite}}. \qquad (9)$$

The exchange interaction matrices are calculated using the relativistic torque method as described in Ref. 29. The sum in Eq. (8) over j can be cast into sums over atomic layers

and over sites within atomic layers. In particular, the latter suffers from convergence problems since $\boldsymbol{J}_{ij}$ decays, at best, as $1/R_{ij}^3$, where R_{ij} denotes the distance between atoms i and j. For this reason the corresponding sum was transformed into an integral in k space, the convergence of which could easily be controlled; for details see Ref. 29. We again note that, due to two-dimensional (2D) translational invariance, d_i and $K_{i,\text{intersite}}$ are the same for all sites i in a given layer, therefore, in the following we shall use them as layer-resolved quantities.

III. RESULTS

A. Local spin and orbital moments

The calculated atomic spin moments are plotted in Fig. 3, displaying a fairly similar picture for the two systems A and B. In the interior of the FePt slab the moments $m_{\text{Fe}}^{(\text{FePt})} = 2.86\mu_{\text{B}}$ and $m_{\text{Pt}}^{(\text{FePt})} = 0.32\mu_{\text{B}}$ are close to their bulk values in FePt. Moreover, the Fe moments approach their bulk Fe value at the edges of region I. Nevertheless, we observe that the bulk Fe spin moment is slightly enhanced in system B, $m_{\text{Fe}}^{(\text{Fe,B})} = 2.07\mu_{\text{B}}$, as compared to system A, $m_{\text{Fe}}^{(\text{Fe,A})} = 1.97\mu_{\text{B}}$. This difference is most likely due to the slight tetragonality of the Fe unit cell along the z direction (and the associated increase in volume) as discussed above for system B. An apparent difference between the spin moments of systems A and B occurs at the interface: Although the Fe moments at the interface $m_{\pm 9}$ are slightly increased in system A, for system B the enhancement of these moments is more pronounced. Moreover, unlike in system A, in system B the spin moments in layer 10, $m_{\pm 10}$, are also enhanced. This means that, as expected, the transition of the moments from bulk Fe to bulk FePt is smoother in the relaxed case.

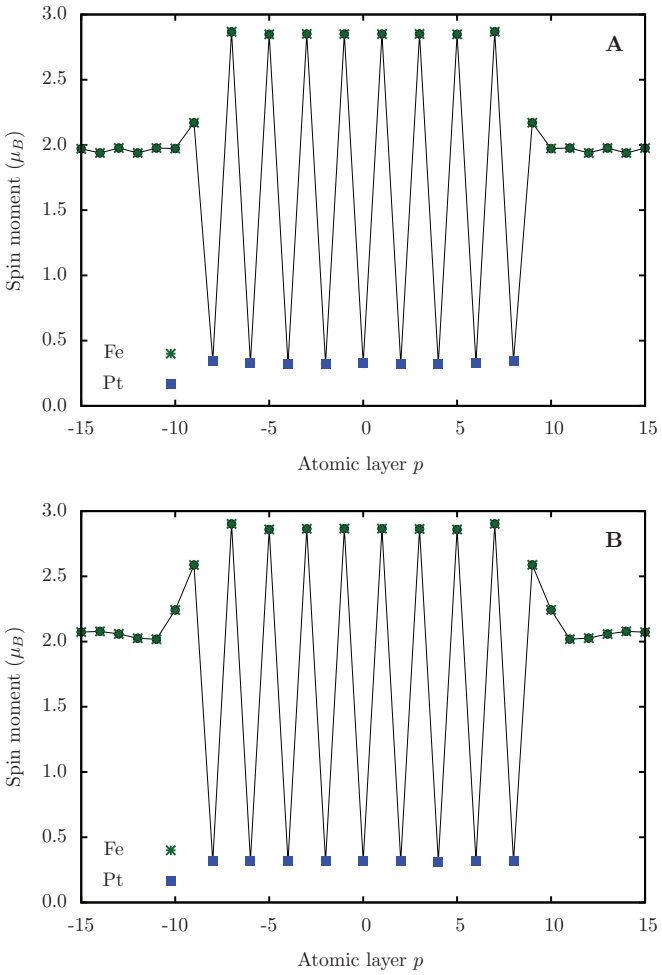

FIG. 3. (Color online) Calculated layer-resolved spin moments (green ∗, Fe; blue ■, Pt) for systems A and B. Solid lines serve as guides for the eye.

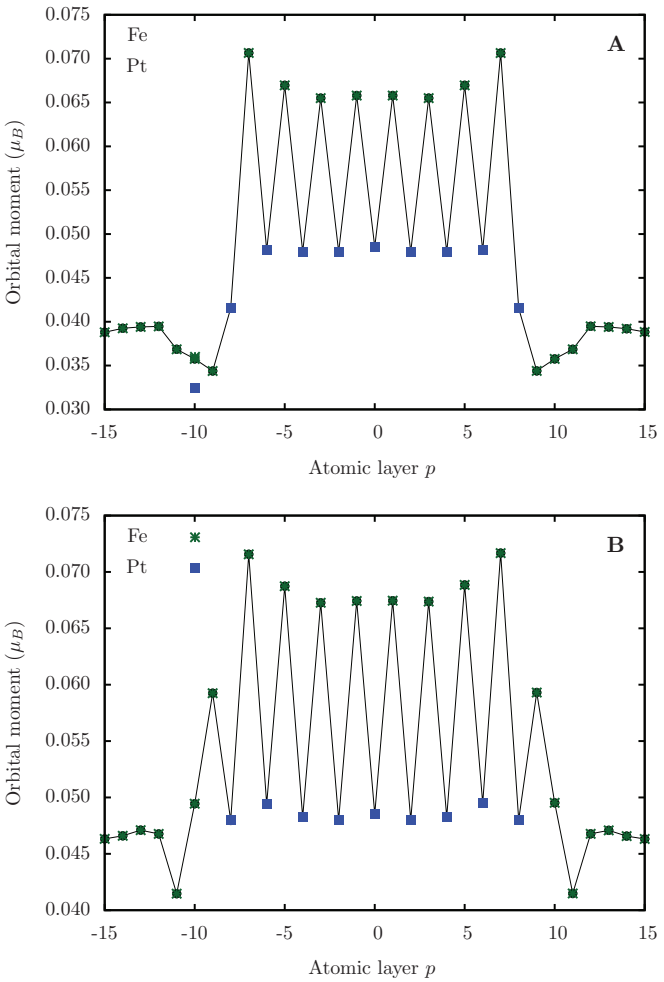

FIG. 4. (Color online) Calculated layer-resolved orbital moments (green ∗, Fe; blue ■, Pt) for systems A and B. Solid lines serve as guides for the eye.

Using the relativistic SKKR method, the local orbital moments can also be calculated. These values are displayed in Fig. 4 across the Fe/FePt/Fe system. Though much smaller in magnitude, the orbital moments are more strongly affected by the presence of the Fe/FePt interface than the spin moments. For example, for both systems we observe a 10% increase in the Fe orbital moment from $0.065\mu_B$ at the center of the FePt phase to $0.072\mu_B$ at the interface. The orbital moments in the Fe bulk region of system B exhibit large changes, reaching nearly $0.060\mu_B$ in the interfacial Fe layer $p = \pm 9$, opposed to the decreased value of $0.033\mu_B$ in system A. With regard to the orbital moments related to the Pt sites, in system B a small oscillation around $m_{\text{Pt}}^{(\text{orb})} \approx 0.048\mu_B$ is observed. In system A

the oscillation of the Pt orbital moment inside the FePt slab is negligible, however, at the interface Pt layer $p = \pm 8$ the orbital moment drops from $0.048\mu_B$ to $0.042\mu_B$.

B. Exchange interactions

Figures 5 and 6 show typical Fe-Fe isotropic exchange interactions J_{ij} in systems A and B, respectively, as a function of the distance R_{ij}. Here we fixed sites i in three different atomic layers: in layers ± 13, which are representative for Fe bulk; in layers ± 1, characteristic of bulk FePt; and in the interfacial Fe layers ± 9. Furthermore, we displayed separately the interactions between Fe atoms within the same layer (intralayer) and in different layers (interlayer).

The Fe bulk region in system A is governed by large ferromagnetic nearest-neighbor (NN) interactions [see Fig. 5(a)]. Due to the bcc(001) geometry, these interactions correspond to interlayer pairs, while the next-nearest-neighbor (NNN) interactions to both interlayer and intralayer pairs. The degeneracy of the eight NN interactions is obviously lifted according to site j being in layers ± 14 and ± 12 since the system has no mirror symmetry with respect to layers ± 13. The same applies to the six NNN interactions, for which the lifting is threefold, namely, for sites j in layers ± 14, ± 13, and ± 12. Similar lifting of degeneracies can also be seen for more distant pairs. The tetragonal expansion of the bcc structure for system B [see Fig. 6(a)] clearly shows up in a drastic increase of the interlayer NNN interactions, while the NN interactions are slightly reduced. Apparently, the intralayer Fe-Fe interactions are only slightly influenced by the tetragonal distortion.

The NN and NNN intralayer Fe-Fe interactions in the FePt slab are strongly ferromagnetic [see Fig. 5(b)]. While the NN and NNN interlayer interactions are also ferromagnetic, the Fe-Fe interlayer coupling in this region is governed by the large antiferromagnetic third NN interaction. Thus, considering only Fe-Fe interactions, the FePt slab would have a layered antiferromagnetic ordering, i.e., ferromagnetic within the Fe layers and antiferromagnetic between layers. However, the relatively large ferromagnetic NN Fe-Pt interactions (5 meV) stabilize a ferromagnetic ordering for the FePt slab. We note that the magnetic ordering of FePt sensitively depends on the c/a ratio and on the long-range chemical disorder of the Fe and Pt components.[30] Since the geometry of the FePt slab is nearly the same in systems A and B, the corresponding Fe-Fe interactions are also very similar for the two systems [compare Figs. 5(b) and 6(b)].

The exchange interactions of an Fe atom in the interfacial layers ± 9 to other Fe atoms appear to be a combination of those in the Fe bulk and in the FePt slab, but distinct differences can also be seen. As can be inferred from Fig. 5(c), in system A the strong ferromagnetic NN interlayer interactions to the Fe side (layers ± 10) are reduced by about 10 meV, however, the NNN interlayer interaction is dramatically increased. The interlayer couplings to the Fe layers in the FePt slab maintain their dominating antiferromagnetic character. The intralayer Fe-Fe interactions take mostly positive, but very small values. The effects of the geometry relaxation can be seen in the remarkable enhancement of the NNN interlayer Fe-Fe interaction (from 20 meV to 34 meV) and also in an increase of the intralayer interactions up to a distance of $2a_{2D}$.

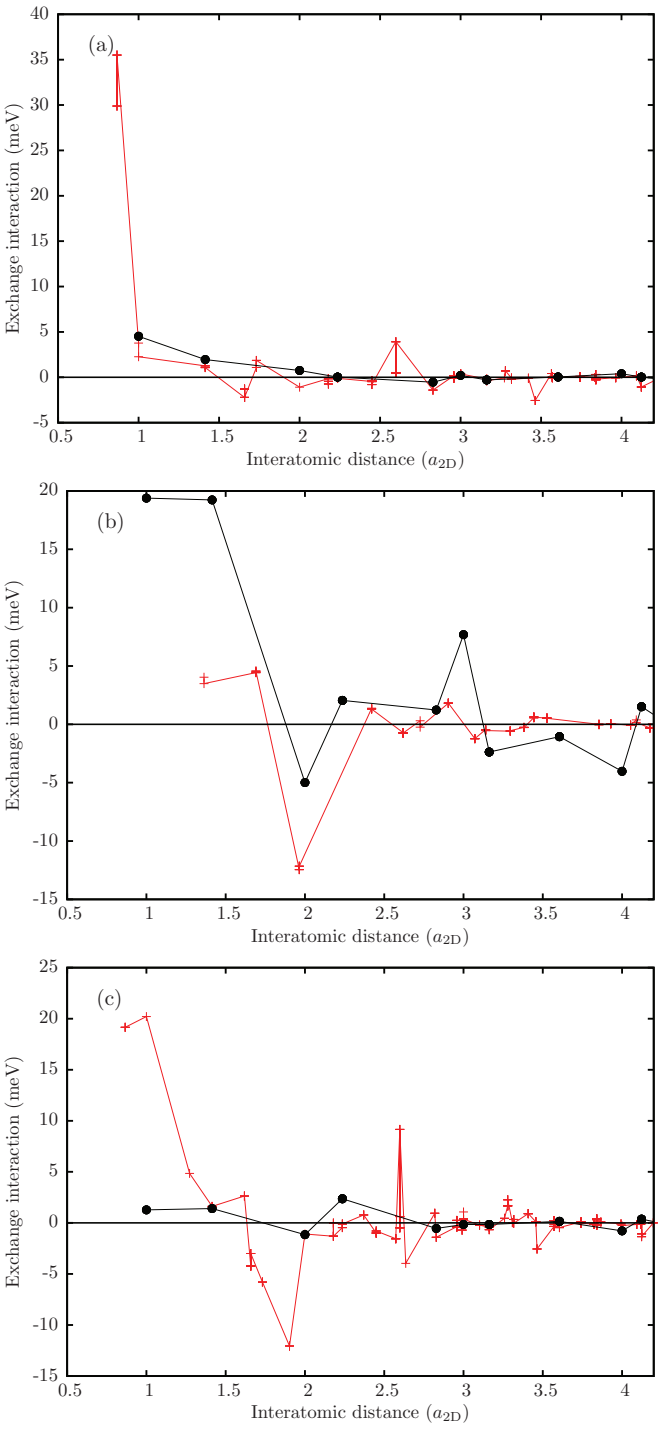

FIG. 5. (Color online) Calculated Fe-Fe isotropic exchange interactions J_{ij} for system A as functions of atomic distance with site i (a) in the bulklike Fe layers $p = \pm 13$, (b) in Fe layers in the FePt slab $p = \pm 1$, and (c) in the interfacial Fe layers $p = \pm 9$. We distinguish in-plane Fe-Fe interactions (black •) and out-of-plane Fe-Fe interactions (red +). Solid lines serve as guides for the eye.

In order to characterize the strength of the isotropic exchange interactions in a magnetic system, effective exchange parameters are often used, defined for a given site i as

$$J_i = \sum_{j\,(\neq i)} J_{ij}. \tag{10}$$

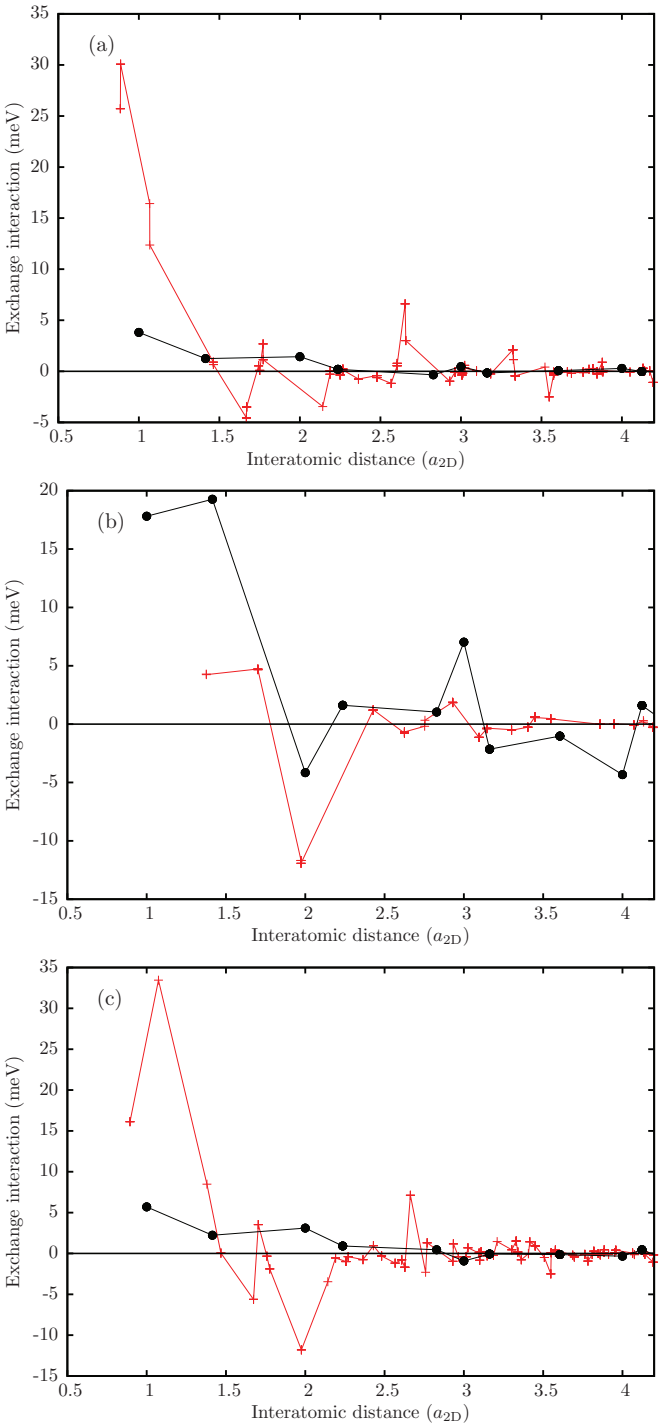

FIG. 6. (Color online) Same as Fig. 5 but for system B.

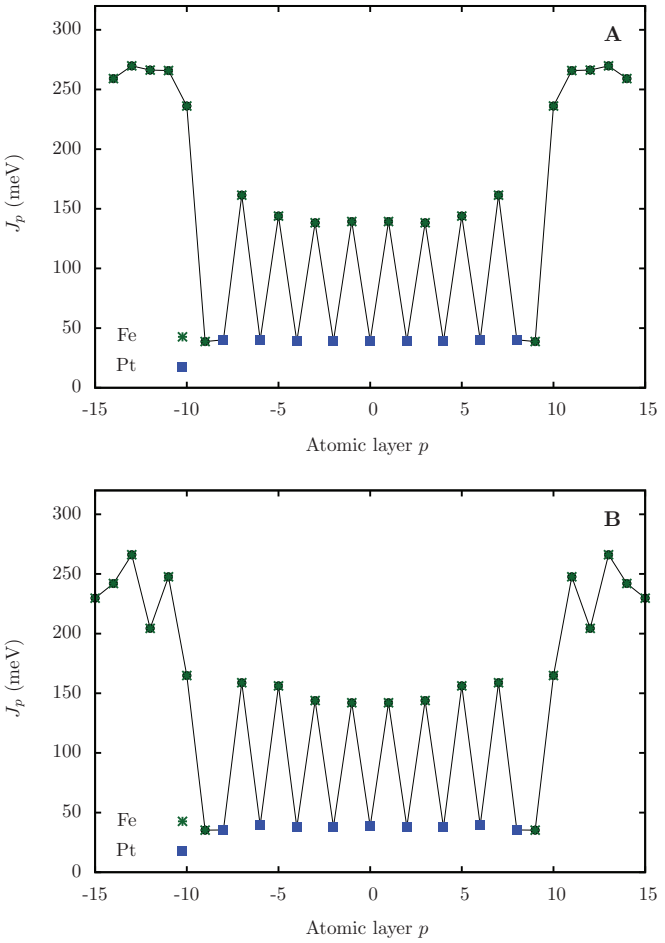

FIG. 7. (Color online) Calculated layer-resolved effective isotropic exchange constants J_p [see Eq. (10)] for systems A and B. The blue ■ and green ∗ represent J_p for Pt and Fe layers, respectively. Solid lines serve as guides for the eye.

For a 2D translationally invariant system, J_i must of course be identical for each site in a given layer. Therefore, in the following, we shall label them by layer indices p. For systems A and B, we calculated J_p by considering all neighbors within a distance of seven a_{2D}, which ensured a reliable convergence of the sum in Eq. (10). The calculated layer-resolved effective exchange parameters are plotted in Fig. 7 for systems A and B.

Within the FePt slab, the effective exchange interactions of systems A and B exhibit very similar layer-resolved behaviors. The value of J_p for the Fe layers is about 150 meV in the center of the FePt slab and is slightly enhanced at the edges of the slab (i.e., towards layers $p = \pm 7$). This is mainly a consequence of an enhancement of the ferromagnetic NN intralayer Fe-Fe interaction towards the outer layers of the FePt slab. The effective exchange parameter of about 40 meV observed in the Pt layers stems mainly from the strongly ferromagnetic nearest-neighbor Fe-Pt interactions.

The (soft) Fe part of the system is characterized by much larger effective exchange $J_p \sim 260$ meV. This high value of the effective exchange parameter is a highly important property of the soft magnet part in exchange-coupled magnetic recording media as it enables the lever effect in switching the magnetization of the hard (FePt) phase. It should be noted that the effective exchange parameters calculated for the interior of the FePt slab and the Fe bulk part of the system correspond to mean-field Curie temperatures of $T_C^{FePt} \sim 700$ K and $T_C^{Fe} \sim 1000$ K, in good agreement with the corresponding experimental values.[31,32]

Approaching the Fe/FePt interface from region I, the effective exchange of the Fe layers drops rapidly and the interfacial Fe layers $p = \pm 9$ exhibit an effective exchange of merely ∼40 meV, almost identical to the effective exchange of the Pt

layers. This reduction of J_p originates in the weak intralayer couplings in layers $p = \pm 9$ and the mostly antiferromagnetic coupling of this layers with the hard layers $|p| \leqslant 7$, largely compensating for the NN and NNN ferromagnetic interactions to the soft layers $|p| \geqslant 10$ [see Fig. 5(c)]. Our results for the effective exchange parameters in the unrelaxed system A are in satisfactory agreement with those in Ref. 13, although in that work significantly smaller magnitudes of J_p are reported as compared to the values presented here.

Interestingly, in system A, the effective exchange of the Fe layer $p = \pm 10$ $J_{\pm 10} \sim 230$ meV, i.e., it almost recovers the bulk value. In contrast, in system B, $J_{\pm 10}$ remains remarkably small ($\sim$160 meV). Also, in system B the effective exchange exhibits relatively large fluctuations throughout the Fe layers $|p| \geqslant 10$. These differences could be attributed to the fact that the geometry of the Fe bulk is different for the two systems (see Sec. II). Although the oscillations can be seen for all the interactions of these Fe layers, the strongest contribution to the oscillatory behavior comes from the ferromagnetic NN out-of-plane interactions. This is to be expected as the variation in the interlayer distance (due to the geometrical relaxation) mostly affect the hybridization between orbitals centered at adjacent atomic layers.

C. Magnetocrystalline anisotropy energy

Figure 8 shows the layer-resolved MAE contributions K_p [see Eq. (2)] for systems A and B. The MAE contributions of the Fe layers in the FePt slab oscillate between about 2.5 meV and 3 meV. The frequency and the magnitude of these oscillations are different for the two systems, most probably due to the different boundary conditions. In system B, due to the evidently smaller amplitude of oscillation, K_i^{Fe} settles more quickly around the bulk value of 3 meV. In both systems, K_i of all the Pt layers is very small, $\sim$0.2 meV. In the Fe parts of the system K_i^{Fe} quickly approaches (practically) zero since the MAE of Fe bulk is on the order of μeV. Note that for system B, the Fe bulk has a tetragonal distortion of 6%, however, this generates only a very small MAE of 0.05 meV.

It should be recalled that the site resolution of the MAE is based on the site-projected DOS. As demonstrated also by Burkert *et al.*,[33] for ordered FePt this construction leads to a dominating contribution of the Fe atoms, while the Pt atoms contribute only about 30% to the MAE. Remarkably, our relativistic SKKR calculations yield a considerably lower ($<$10 %) contribution of Pt. Since the site-resolved MAE contributions have been shown to depend sensitively on the band filling,[33] the differences in the electronic structure methods (in Ref. 33 the full potential linear muffin-tin orbital method was used) can easily explain this difference in the site-resolved MAE contributions. Moreover, our concept of site resolution (and that in Ref. 33) may appear confusing with respect to that of Refs. 27 and 28, where the largest contribution to the MAE comes from the Pt sites, in line with the large spin-orbit coupling of Pt. There is, however, no confusion concerning the two types of site resolutions since in nonperturbative calculations such as ours the spin-orbit interaction on the Pt atoms is transferred to the electronic states at the Fe sites due to the strong $3d$ Fe–$5d$ Pt hybridization.[33]

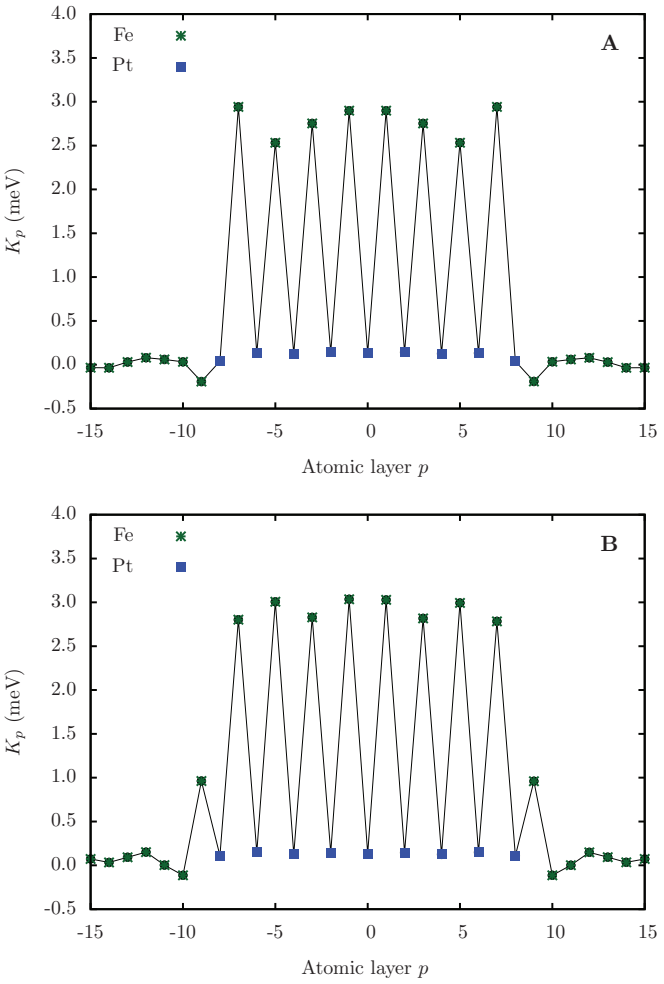

FIG. 8. (Color online) Calculated layer-resolved contributions to the MAE K_p (blue ■, Pt; green $*$, Fe) for systems A and B. Solid lines serve as guides for the eye.

As a remarkable difference between systems A and B, in system B the Fe layers at the interface (layers ± 9) exhibit a contribution of about 1 meV to the MAE, while in system A this contribution is even negative (~ -0.25 meV). In order to gain an understanding of this difference, we tried applying Bruno's arguments in terms of second-order perturbation theory.[34,35] To this end, we performed self-consistent scalar-relativistic calculations (i.e., calculations in which the spin-orbit coupling is excluded) and calculated the local partial density of states (LPDOS). In Fig. 9 we plotted the d-like spin- and orbital-resolved LPDOS at layer 9. The LPDOS clearly shows a strong spin polarization (almost filled majority-spin band) in this layer, which is a necessary condition to apply Bruno's theory. Apparently, the d_{z^2} LPDOS is nearly insensitive to the geometry relaxation, while upon relaxation a considerable weight of the $d_{xz,yz}$ LPDOS (and, to some extent, also of the d_{xy,x^2-y^2} LPDOS) is shifted towards the Fermi level in the occupied regime in both spin channels. The unoccupied part of the minority-spin channel of these orbital-resolved states is also affected by the geometrical relaxation. However, in the vicinity of the Fermi level only a small increase in the unoccupied minority-spin LPDOS occurs. (The majority-spin LPDOS clearly decreases at the Fermi level, but it is not

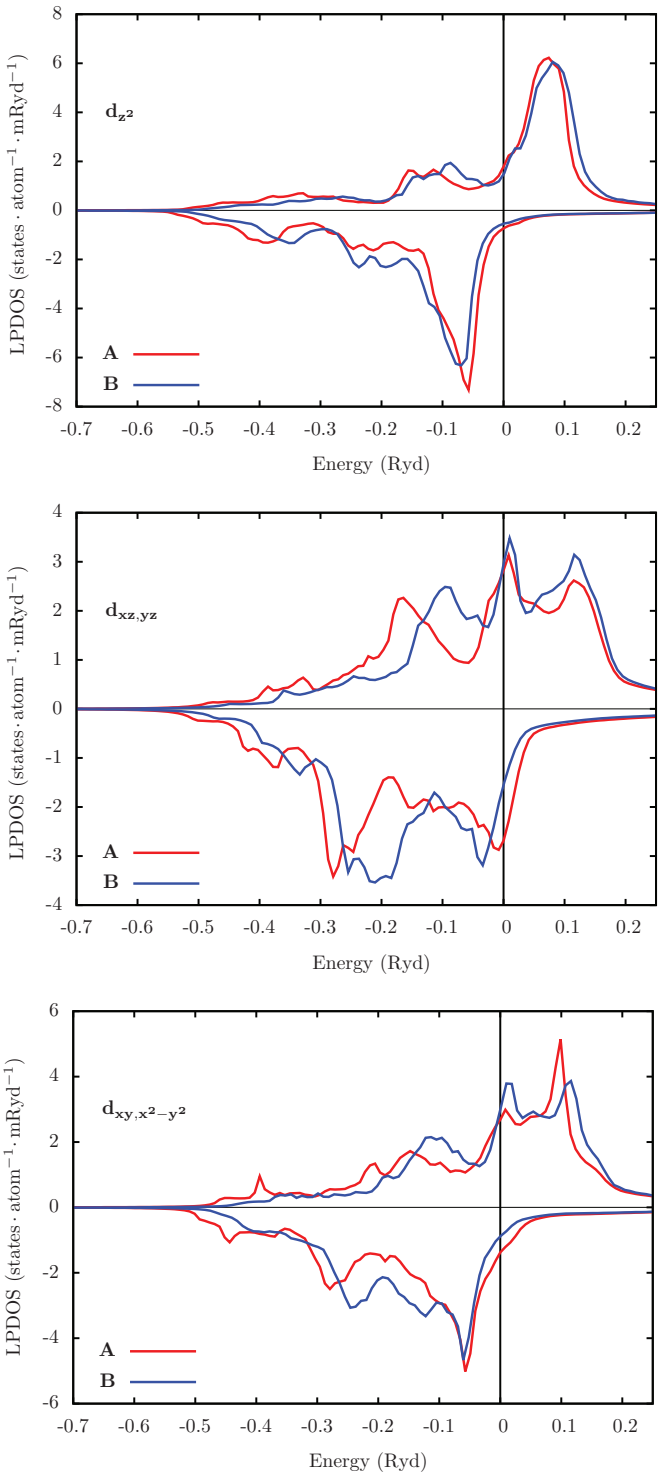

FIG. 9. (Color online) Calculated d-like spin- and orbital-resolved local partial densities of states (LPDOS) for layer 9: d_{z^2} ($m = 0$) (top), d_{xz} and d_{yz} ($m = \pm 1$) (middle), d_{xy} and $d_{x^2-y^2}$ ($m = \pm 2$) (bottom). Positive/negative values stand for the minority/majority spin channels. The zero of the energy is shifted to the Fermi energy.

relevant in our present theoretical estimation.) Since the spin-orbit interaction gives rise to couplings between the d_{xz} and d_{yz} states, inducing a perpendicular MAE, as well as to couplings between the $d_{xz,yz}$ and d_{z^2} states, inducing an in-plane MAE,[35] it is hardly possible to identify a well-established difference in

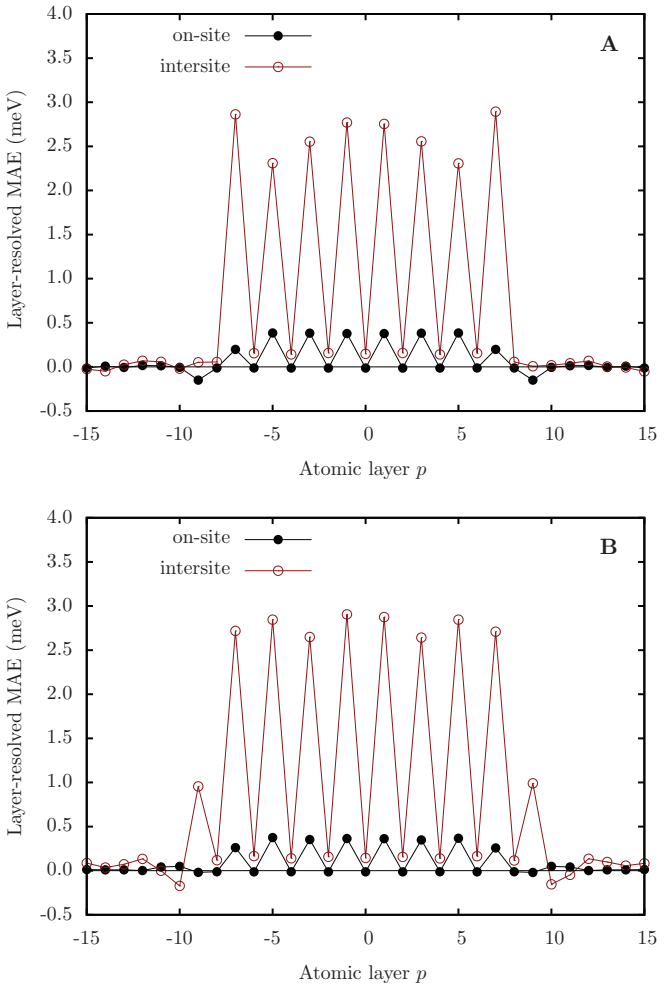

FIG. 10. (Color online) Calculated layer-resolved on-site (●) and intersite (○) anisotropies for systems A and B [see Eq. (9)]. Solid lines serve as guides for the eye.

the specific local contribution to the MAE regarding the two systems.

In terms of the localized-spin model as described in Sec. II, the MAE can be cast into on-site and intersite contributions as per Eq. (9). Although the microscopic model to construct an anisotropic spin model differs from the one used in this work, the results of Mryasov *et al.*[28] strongly suggest that the MAE of the FePt systems arises mainly from effective Fe-Fe intersite interactions [Eq. (7)] mediated by the spin-orbit coupling on the Pt atoms. Mapping our results on the MAE to the spin model [see Eqs. (5)–(9)] provides a unique opportunity to check the assertion of Ref. 28. Using the methods introduced in Ref. 29, we calculated the on-site and intersite parts of the layer-resolved MAE related to an extended Heisenberg spin model and plotted these contributions in Fig. 10.

Inspecting Fig. 10 it is indeed obvious that approximately 90% of the MAE of FePt is associated with anisotropic intersite interactions between Fe atoms. The shape of the $K_{p,\text{intersite}}$ across the atomic layers p coincides reasonably well with that of K_p presented in Fig. 8. The on-site anisotropies are quite stable on the Fe sites within the FePt slab and practically vanish at the Pt sites. Furthermore, the increase in K_p at the Fe/FePt interface (i.e., in layers $p = \pm 9$) due to relaxation stems

mostly from the intersite anisotropy. Using the arguments of Mryasov *et al.*,[28] this can be explained in terms of the electron scattering between these Fe atoms and the Pt atoms in the adjacent layer $p = \pm 8$, experiencing thus large spin-orbit coupling. Interestingly, in system A this induced anisotropy effect is suppressed and the small negative contribution to the MAE in these layers is of on-site origin. Remarkably, Eq. (9) is satisfied with good accuracy if K_p is taken from the direct calculation via the torque method. This lends substantial credit to the use of the tensorial exchange interactions in spin-dynamics simulations.

As a final step in our *ab initio* investigations, we address the question of how much the MAE of the finite FePt slab changes with respect to the bulk MAE related to an FePt layer of the same size. Clearly, this point has a crucial technological impact, namely, whether the perpendicular MAE can be increased by forming an Fe/FePt multilayer sequence. Regarding Fig. 8, it is obvious that for the chosen width of the FePt layer the effect of a single interface can hardly be separated since the oscillations of K_p indicate a strong interaction between the two Fe/FePt interfaces (quantum interference effects). Thus we define the excess MAE generated by the entire FePt slab as

$$\Delta K_{\text{FePt slab}} = \sum_{p=-15}^{15} K_p - 9K_{\text{FePt}}, \tag{11}$$

where in the sum we also include layers from the Fe part of the system. Note that the MAE of Fe bulk (on the order of μeV/atom) is neglected and K_{FePt} is the MAE per formula unit (f.u.) for bulk FePt. We calculated $K_{\text{FePt}} = 3.37$ meV/f.u., which, although high in comparison to experiment, is in good agreement with other theoretical results based on the LSDA or the LSDA + U approach.[36,37]

When evaluating $\Delta K_{\text{FePt slab}}$ we needed to consider that for systems A and B the Fermi level of bulk Fe is used instead of the Fermi level of bulk FePt, which slightly affects the value of K_{FePt} calculated within the SKKR ASA approach. In order to calibrate K_{FePt} we used system C [an unrelaxed Fe/FePt/Fe trilayer immersed in FePt bulk (see Sec. II)]. Indeed, in the FePt slab of system C the shape we obtained for K_i across the atomic layers was very similar to that for system A, while for the innermost FePt layers the bulk MAE K_{FePt} was retained to within less than 1% numerical accuracy. Since the corresponding MAE contributions in system A are smaller by 0.33 meV/f.u., in Eq. (11) we used a corrected value of 3.04 meV/f.u. for K_{FePt}.

For system A, we obtain a reduction in the total MAE, $\Delta K^{\text{A}}_{\text{FePt slab}} \approx -4.2$ meV. This reduction stems primarily from the interfacial layers $i = \pm 9$ (see Fig. 8). From this figure it is obvious that the contribution of one Fe layer to the MAE of the FePt slab is missing since this Fe layer becomes much rather an interfacial Fe layer. Upon relaxation, i.e., in system B, the interfacial Fe layers have remarkably enhanced contributions to the MAE (see Fig. 8) as these Fe layers seem to belong rather to the FePt slab. Moreover, in this case the Fe layers in the FePt slab have contributions to the MAE closer to that in bulk FePt as compared to system A. Consequently, for system B the MAE of bulk FePt is almost entirely retained, $\Delta K^{\text{B}}_{\text{FePt slab}} \approx -0.4$ meV. Comparing this value to the total MAE of the FePt slab immersed in Fe, 26.9 meV, we conclude that the MAE of a realistic $[\text{Fe}_m/(\text{FePt})_k]_n$ ($m \gtrsim 10$, $k \gtrsim 9$) multilayer sequence is approximately equal to the MAE of nk FePt bulk layers.

IV. IMPLICATIONS FOR MESOSCOPIC SPIN STRUCTURES

The detailed mapping of the *ab initio* information onto a spin model, which will allow, for example, calculations of the temperature dependence of the MAE values, is beyond the scope of the current work. Here we give a simple illustration of the implications of the *ab initio* results and their effect on magnetic spin structures and indeed the exchange spring phenomenon. Specifically, we consider the effect of an abrupt change in magnetic properties, especially the MAE, which is known to give rise to pinning of a domain wall at the interface. Kronmüller and Goll[38] developed a micromagnetic model of magnetization reversal in a material consisting of two coupled phases with different magnetic properties. It was found that a domain wall (DW) could be pinned at the interface between the different layers, the pinning being overcome by a critical field

$$H_c = \frac{2K^{\text{II}}}{M_s^{\text{II}}} \frac{1 - \epsilon_K \epsilon_A}{(1 + \sqrt{\epsilon_M \epsilon_A})^2}, \tag{12}$$

where the superscript II refers to the properties of the hard phase and ϵ_K, ϵ_A, and ϵ_M refer to the ratio of the anisotropy constant, the micromagnetic exchange constant, and saturation magnetization, respectively, in the soft and hard phases. The coercivity of the hard phase is invariably reduced by all combinations of material parameters.

However, Eq. (12) was derived under the assumption of bulk exchange coupling across the interface and it has been shown by Guslienko *et al.*[39] that the exchange spring effect is strongly dependent on the degree of coupling at the interface. In Ref. 39 the interface coupling was taken as a variable, but the *ab initio* calculations presented here allow us to study the exchange spring phenomenon with no fitting parameters. We use a simple spin-chain model as in Ref. 39, treating the low-exchange layer as an interface providing a weakened exchange between the FePt and Fe layers. Within each layer we can write down the spin Hamiltonian

$$\mathcal{H} = -J \sum_{i,j(\text{NN})} \vec{S}_i \cdot \vec{S}_j + \sum_i K \left(S_i^z\right)^2 - \sum_i \mu \vec{H} \cdot \vec{S}_i, \tag{13}$$

where J is the intralayer nearest-neighbor exchange coupling, $\vec{S}_i$ the unit vector representing the spin direction, K the anisotropy constant, μ the atomic spin in the given layer, and $\vec{H}$ the applied field.

We allow for reduced exchange coupling at the interfaces by writing the exchange energy between interface spins as

$$\mathcal{H}_{\text{int}} = -J_{\text{int}} \sum_{i,j} \vec{S}_i \cdot \vec{S}_j, \tag{14}$$

where the spins i, j are in separate layers. Similar to the case of the $IrMn_3$/Co (111) system in Ref. 18, our calculations show sizable DM interactions near the interface. Due to the $C4v$ symmetry, however, the DM energy cancels for the Néel walls to be investigated in the following. For that reason, we neglected the DM interactions in our model of

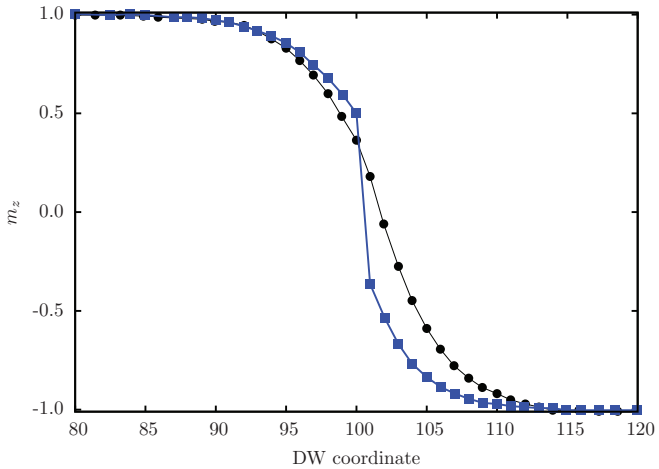

FIG. 11. (Color online) Calculated domain wall structures prior to magnetization reversal for fully exchange coupled layers (black •) and layers coupled with *ab initio* exchange parameters for the relaxed system B (blue ■). The relaxed system shows a discontinuous DW structure due to the weak interlayer exchange coupling.

Eq. (14). The equilibrium state of the spin system is determined by integrating the Landau-Lifshitz equation, without the precession term

$$\frac{d\vec{S}_i}{dt} = -\alpha \vec{S}_i \times (\vec{S}_i \times \vec{H}_i), \tag{15}$$

with $\vec{H}_i$ being the effective field acting on spin i.

Figure 11 shows calculated DW structures prior to magnetization reversal for fully exchange-coupled layers and layers coupled with *ab initio* exchange parameters for the relaxed system. In the latter case the interlayer exchange is approximately 20% of the bulk exchange of FePt. The associated coercivities are 5.9 and 7.24 T, respectively, reduced from the bulk coercivity of 14 T due to the exchange spring effect. For the bulk interlayer exchange case the DW width in the Fe layer is considerably smaller than the usual expectation due to the presence of the large applied field. Nonetheless, the DW is continuous across the interface, in contrast to the case of the reduced exchange of the relaxed microstructure. The effect of the reduced exchange on the coercivity is relatively weak, consistent with the results given in Ref. 39. However, even relatively small changes can be significant for the design and operation of practical recording media.

V. CONCLUSION

We have presented first-principles calculations of the exchange interactions and the magnetocrystalline anisotropy energy in an Fe/FePt/Fe sandwich system. In particular, we investigated how the geometrical relaxation influences the calculated magnetic properties of the system. In accordance with previous work on an unrelaxed Fe/FePt/Fe system,[13] we found a dramatic reduction in the exchange coupling between the Fe layers at the Fe/FePt (soft/hard) interface. Moreover, in the relaxed system, these layers add a remarkable positive contribution to the MAE. From the tensorial exchange interactions evaluated by means of the relativistic torque method,[29] we have shown that the MAE of the FePt slab and the interface MAE are dominated by anisotropic intersite exchange interactions. Moreover, our calculations indicate that the formation of an Fe/FePt layer sequence reduces the perpendicular MAE. In the case of a relaxed geometry, which we consider to be relevant to a multilayer system, this reduction is slight, on the order of ∼0.4 meV per FePt slab.

We also show that the *ab initio* parameters will have a bearing on the mesoscopic spin structures predicted by atomistic and micromagnetic models. Specifically, the reduced exchange coupling between FePt and Fe layers gives rise to a discontinuous spin structure across the FePt/Fe interface. Although the exchange spring effect still gives rise to a large coercivity reduction, it is likely that the discontinuous spin structure could affect the magnetization dynamics. The reduced exchange could also affect the temperature dependence of the interface MAE values, which could also have a significant bearing on the magnetic properties. Both factors require the development of a detailed mapping onto an atomistic spin model. Further, each material combination in a magnetic nanostructure will have interface properties that may differ significantly from the bulk, making further *ab initio* studies of interface properties important in terms of the understanding of the underlying physics of static and dynamic magnetic properties.

ACKNOWLEDGMENTS

Financial support was provided by the Hungarian National Research Foundation (under Contracts No. OTKA 77771 and No. OTKA 84078) and by the New Széchenyi Plan of Hungary (Project No. TÁMOP-4.2.2.B-10/1-2010-0009). Support of the EU under FP7 Contract No. NMP3-SL-2012-281043 FEMTOSPIN is gratefully acknowledged. C.J.A. is grateful to EPSRC for the provision of a research studentship.

[1] D. Suess, J. Lee, J. Fidler, and T. Schrefl, J. Magn. Magn. Mater. **321**, 545 (2009).
[2] R. Skomski and J. M. D. Coey, Phys. Rev. B **48**, 15812 (1993).
[3] C. T. Pan and S. C. Shen, J. Magn. Magn. Mater. **285**, 422 (2005).
[4] F. Casoli, F. Albertini, L. Nasi, S. Fabbrici, R. Cabassi, F. Bolzoni, C. Bocchi, and P. Luches, Acta Mater. **58**, 3594 (2010).
[5] D. Makarov, J. Lee, C. Brombacher, C. Schubert, M. Fuger, D. Suess, J. Fidler, and M. Albrecht, Appl. Phys. Lett. **96**, 062501 (2010).
[6] A.-C. Sun, F.-T. Yuan, J.-H. Hsu, Y. H. Lin, and P. C. Kuo, IEEE Trans. Magn. **45**, 2709 (2009).
[7] D. C. Crew, J. Kim, L. H. Lewis, and K. Barmak, J. Magn. Magn. Mater. **233**, 257 (2001).
[8] J. S. Jiang, J. E. Pearson, Z. Y. Liu, B. Kabius, S. Trasobares, D. J. Miller, S. D. Bader, D. R. Lee, D. Haskel, G. Srajer, and J. P. Liu, Appl. Phys. Lett. **85**, 5293 (2004).
[9] F. Casoli, F. Albertini, S. Fabbrici, C. Bocchi, L. Nasi, R. Ciprian, and L. Pareti, IEEE Trans. Magn. **41**, 3877 (2005).

[10]F. Casoli, F. Albertini, L. Nasi, S. Fabbrici, R. Cabassi, F. Bolzoni, and C. Bocchi, Appl. Phys. Lett. **92**, 142506 (2008).
[11]G. Varvaro, F. Albertini, E. Agostinelli, F. Casoli, D. Fiorani, S. Laureti, P. Lupo, P. Ranzieri, B. Astinchap, and A. M. Testa, New J. Phys. **14**, 073008 (2012).
[12]E. Kneller and R. Hawig, IEEE Trans. Mag. **27**, 3588 (1991).
[13]R. Sabiryanov and S. Jaswal, J. Magn. Magn. Mater. **177–181**, 989 (1998).
[14]M. D. Segall, P. J. D. Lindan, M. J. Probert, C. J. Pickard, P. J. Hasnip, S. J. Clark, and M. C. Payne, J. Phys.: Condens. Matter **14**, 2717 (2002).
[15]M. C. Payne, M. P. Teter, D. C. Allan, T. A. Arias, and J. D. Joannopoulos, Rev. Mod. Phys. **64**, 1045 (1992).
[16]S. J. Clark, M. D. Segall, C. J. Pickard, P. J. Hasnip, M. J. Probert, K. Refson, and M. C. Payne, Z. Kristallogr. **220**, 567 (2005).
[17]J. Zabloudil, R. Hammerling, L. Szunyogh, and P. Weinberger, *Electron Scattering in Solid Matter* (Springer, Berlin, 2005).
[18]L. Szunyogh, L. Udvardi, J. Jackson, U. Nowak, and R. Chantrell, Phys. Rev. B **83**, 024401 (2011).
[19]R. Yanes, J. Jackson, L. Udvardi, L. Szunyogh, and U. Nowak, arXiv:1305.2308.
[20]I. Dzyaloshinskii, J. Phys. Chem. Solids **4**, 241 (1958).
[21]T. Moriya, Phys. Rev. **120**, 91 (1960).
[22]P. J. Hasnip and C. J. Pickard, Comput. Phys. Commun. **174**, 24 (2006).
[23]S. H. Vosko, L. Wilk, and M. Nusair, Can. J. Phys. **58**, 1200 (1980).
[24]H. J. F. Jansen, Phys. Rev. B **59**, 4699 (1999).
[25]X. Wang, R. Wu, D. S. Wang, and A. J. Freeman, Phys. Rev. B **54**, 61 (1996).
[26]J. B. Staunton, L. Szunyogh, A. Buruzs, B. L. Gyorffy, S. Ostanin, and L. Udvardi, Phys. Rev. B **74**, 144411 (2006).
[27]I. V. Solovyev, P. H. Dederichs, and I. Mertig, Phys. Rev. B **52**, 13419 (1995).
[28]O. N. Mryasov, U. Nowak, K. Y. Guslienko, and R. W. Chantrell, Europhys. Lett. **69**, 805 (2005).
[29]L. Udvardi, L. Szunyogh, K. Palotás, and P. Weinberger, Phys. Rev. B **68**, 104436 (2003).
[30]G. Brown, B. Kraczek, A. Janotti, T. C. Schulthess, G. M. Stocks, and D. D. Johnson, Phys. Rev. B **68**, 052405 (2003).
[31]K. Barmak, J. Kim, D. C. Berry, K. W. Wierman, E. B. Svedberg, and J. K. Howard, J. Appl. Phys. **95**, 7486 (2004).
[32]H. E. Hall and J. R. Hook, *Solid State Physics 2E* (Wiley, Chichester, 1991).
[33]T. Burkert, O. Eriksson, S. I. Simak, A. V. Ruban, B. Sanyal, L. Nordström, and J. M. Wills, Phys. Rev. B **71**, 134411 (2005).
[34]P. Bruno, Phys. Rev. B **39**, 865 (1989); in *24. Ferienkurse des Forschungszentrum Jülich, 1993*, edited by P. H. Dederichs, P. Grünberg, and W. Zinn (Forschungszentrum Jülich, Jülich, Germany, 1993).
[35]B. Ujfalussy, L. Szunyogh, P. Bruno, and P. Weinberger, Phys. Rev. Lett. **77**, 1805 (1996).
[36]J. Lyubina, I. Opahle, K.-H. Müller, O. Gutfleisch, M. Richter, M. Wolf, and L. Schultz, J. Phys.: Condens. Matter **17**, 4157 (2005).
[37]A. B. Shick and O. N. Mryasov, Phys. Rev. B **67**, 172407 (2003).
[38]H. Kronmüller and D. Goll, Physica B **319**, 122 (2002).
[39]K. Yu. Guslienko, O. Chubykalo-Fesenko, O. Mryasov, R. Chantrell, and D. Weller, Phys. Rev. B **70**, 104405 (2004).